Impact of a Convectively Forced Gravity Wave Drag Parameterization in NCAR CCM3

HYE-YEONG CHUN AND IN-SUN SONG

Department of Atmospheric Sciences, Yonsei University, Seoul, South Korea

JONG-JIN BAIK

School of Earth and Environmental Sciences, Seoul National University, Seoul, South Korea

YOUNG-JOON KIM

Marine Meteorology Division, Naval Research Laboratory, Monterey, California

(Manuscript received 25 July 2003, in final form 23 February 2004)

ABSTRACT

A parameterization of gravity wave drag forced by subgrid-scale cumulus convection (GWDC) proposed by Chun and Baik is implemented into the National Center for Atmospheric Research Community Climate Model (NCAR CCM3) and its effect on perpetual January and July climate is investigated. The cloud-top gravity wave stress is concentrated in the intertropical convergence zone where persistent deep cumulus clouds exist. The resultant zonal wind acceleration due to the breaking of convectively forced gravity waves is predominantly found in the tropical lower stratosphere with westerly acceleration above cloud top and easterly acceleration just below it. Since the parameterized gravity waves are stationary relative to convective clouds, wave breaking occurs mainly in the tropical lower stratosphere where the zonal wind is weak enough for wave saturation. It is shown that the GWDC parameterization significantly alleviates the systematic model biases of zonal-mean zonal wind and temperature. In particular, excessive easterlies in the tropical stratosphere and excessive cold temperatures in the tropical lower stratosphere are reduced by more than 50% by including the GWDC parameterization. The horizontal wind divergence field in the tropical upper troposphere and lower stratosphere is also significantly improved with the GWDC parameterization.

The impact of the GWDC parameterization extends to mid- to high latitudes through planetary wave activity in the winter hemisphere. The increased amplitude of zonal wavenumber 3 in the January Northern Hemisphere and the increased amplitude of zonal wavenumber 2 in the July Southern Hemisphere lead to significant improvements in model performance. The impact of the GWDC parameterization on Eliassen–Palm (EP) flux divergence forcing by stationary waves is generally opposite to that by transient waves in the extratropics, especially in the Northern Hemisphere wintertime. Hence, the zonal-mean zonal wind change by the GWDC parameterization occurs mainly in the Tropics by direct gravity wave drag forcing.

1. Introduction

Momentum forcing due to the breaking of vertically propagating internal gravity waves is one of the crucial factors to understand the observed zonal-mean flow structure in the middle atmosphere as well as in the lower atmosphere. In general circulation models (GCMs), parameterization of orographically forced gravity wave drag can successfully alleviate systematic model biases such as an excessive westerly jet near the tropopause in the Northern Hemisphere (NH) wintertime and associated excessive cold temperature in the polar region (Palmer et al. 1986; McFarlane 1987). However, systematic model biases still remain in the Southern Hemisphere (SH) and tropical regions where mountains are relatively rare.

Since it was found that a large portion of observed gravity waves in the middle atmosphere are nonstationary (Fritts 1984), cumulus convection has received great attention as a possible source of nonstationary gravity waves. Convectively forced gravity waves may give a significant direct impact in the Tropics where persistent cumulus clouds exist and they can provide a significant amount of momentum forcing for the quasi-biennial oscillation (QBO) in the tropical stratosphere (Sato and Dunkerton 1997; Alexander and Holton 1997; Piani et al. 2000). Convectively forced gravity waves can be equally important in the extratropical regions through

Corresponding author address: Prof. Hye-Yeong Chun, Dept. of Atmospheric Sciences, Yonsei University, Seoul 120-749, South Korea.
E-mail: chy@atmos.yonsei.ac.kr

interactions between the zonal-mean flow, planetary waves, and gravity waves with multiple positive and negative feedbacks (Rind et al. 1988; Chun et al. 2001a).

During the last 20 yr, developing gravity wave drag (GWD) parameterizations for use in large-scale models has been one of the most active research areas. For an overview, refer to Kim et al. (2003). There are basically two types of GWD parameterization methods. The first method is to consider a gravity wave source and calculate momentum flux explicitly. Most orographic gravity wave drag parameterization schemes adopt this method (e.g., Palmer et al. 1986; Pierrehumbert 1986; McFarlane 1987; Shutts 1995; Kim 1996; Lott and Miller 1997). Using this method, parameterization schemes for convectively forced gravity wave drag are proposed by Rind et al. (1988), Kershaw (1995), and Chun and Baik (1998, 2002). Recently, Chun et al. (2001a) implemented Chun and Baik's parameterization (Chun and Baik 1998) into the Yonsei University GCM (YONU GCM). Through perpetual July simulations, they showed that the convectively forced GWD (GWDC hereafter) parameterization successfully alleviates the excessive westerly jet in the SH winter stratosphere that appears in most current GCMs. Gravity waves considered in the parameterization by Chun and Baik (1998, 2002) are stationary relative to moving convective sources.

The second method is the so-called wave spectrum method that includes a wide spectrum of gravity waves existing in the atmosphere. In this method, individual wave modes interacting with mean flow are responsible for the deposition of momentum to the large-scale flow. Since Holton (1982) first attempted to parameterize GWD based upon a linear saturation theory by Lindzen (1981), wave spectrum parameterization schemes have been continually developed (e.g., Hines 1991; Fritts and Lu 1993; Medvedev and Klaassen 1995; Alexander and Dunkerton 1999; Warner and McIntyre 1999) with better understanding of gravity waves and their impact on the middle atmosphere. This development has been accelerated due to the increasing appreciation of the influence of nonstationary gravity waves in the middle-atmosphere dynamics such as QBO (e.g., Scaife et al. 2002).

In this study, we implement the GWDC parameterization proposed by Chun and Baik (1998; CB98 hereafter) into the National Center for Atmospheric Research Community Climate Model (NCAR CCM3; Kiehl et al. 1996) and examine its effect on the atmospheric general circulation. NCAR CCM3 has been widely used for climate research and therefore a further improvement of its performance in simulating climate by including a new physical process is very important. This motivates the present study.

2. GWDC parameterization

The GWDC parameterization scheme proposed by CB98 is implemented into CCM3. Here, only a brief description of the scheme is given in its implementation procedure: (i) Calculate gravity wave stress vector at cloud-top level (subscript ct denotes cloud top)

$$\tau_{ct} = -\frac{\rho_{ct}|\mathbf{u}_{ct}|^2}{N\Delta x}\mathbf{u}_{ct}c_1c_2^2\mu_{ct}^2, \tag{1}$$

$$\mu_{ct} = \frac{gQ_0a_1}{c_pNT|\mathbf{u}_{ct}|^2}, \tag{2}$$

where Q_0/c_p is the subgrid-scale convective heating rate (K s^{-1}), c_p the specific heat at constant pressure, g the gravity, N the buoyancy frequency, T the temperature, $\mathbf{u}_{ct}$ the horizontal wind vector at cloud top, ρ_{ct} the air density at cloud top, Δx the horizontal grid size, a_1 the approximate horizontal scale of effective cloud, which is approximated by $\alpha\Delta x$ (where α is the fractional cloud coverage), and c_1 and c_2 are constants ($c_1 = 1.41$ and $c_2 = -0.38$ are used in the present study) related to the horizontal and vertical structure of the diabatic forcing, respectively. (ii) Calculate wave stress at any level parallel to the wave stress vector at cloud top. (iii) Find wave breaking level based upon the minimum Richardson number including wave effect (Ri_m) [$= \mathrm{Ri}(1 - \mu|c_2|)/(1 + \mu\mathrm{Ri}^{1/2}|c_2|)^2$], where Ri is the local Richardson number. That is, if $\mathrm{Ri}_m < 1/4$, wave breaking occurs. Then, calculate the saturation wave stress based upon the Lindzen's (1981) linear saturation theory. If $\mathrm{Ri}_m \geq 1/4$, there is no wave breaking and wave stress is the same as that at the level below. (iv) Repeat this step at higher levels until the wave stress is zero or the model top is reached. (v) Calculate the deposition of momentum in a convection region for momentum conservation. Further details on the theoretical basis of the GWDC parameterization and the procedure of its implementation into a numerical model can be found in CB98 and Chun et al. (2001a), respectively. Note that gravity waves considered in CB98 have a wide spectrum of horizontal wavenumbers but have zero frequency in a reference frame moving with the convective source. Therefore, gravity waves considered in the present parameterization have a single phase speed, which is zero relative to moving clouds. Since the GWDC parameterization is activated only when and where subgrid-scale convective clouds exist, the spatial and temporal variations of gravity wave activity are taken into account according to those of convective clouds.

3. Model and experimental design

CCM3 is a three-dimensional, global spectral model with T42 horizontal truncation and 18 vertical levels from the surface to 2.5 hPa. The cumulus parameterization scheme, which provides the most important input for the GWDC parameterization, used in CCM3 is that of Zhang and McFarlane (1995). A mountain drag parameterization based upon McFarlane (1987) is included. A detailed description of CCM3 can be found in Kiehl et al. (1996).

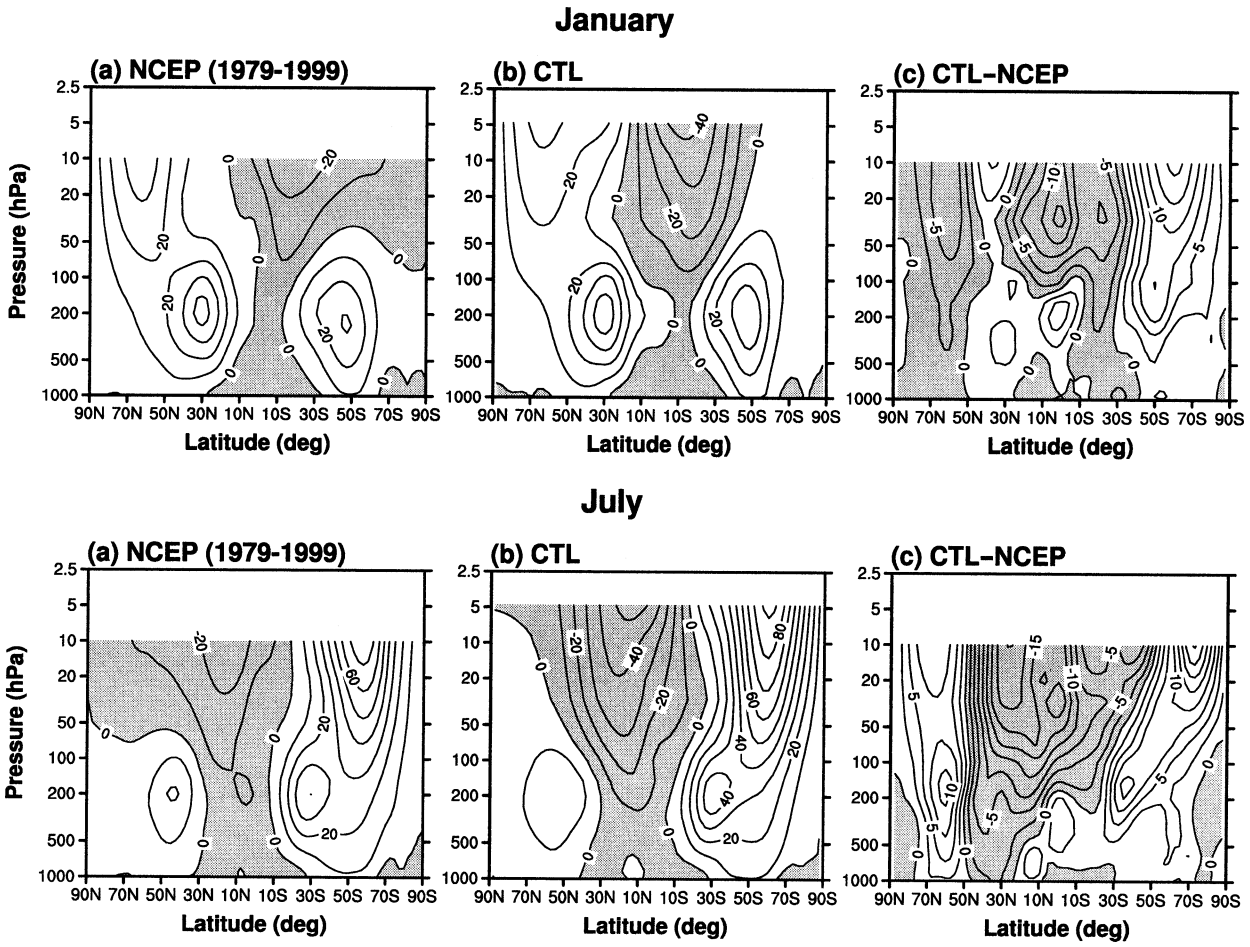

FIG. 1. Zonal-mean zonal wind in (a) NCEP reanalysis data for 21 yr (1979–99), (b) control (CTL) simulation without the GWDC parameterization, and (c) difference between CTL simulation and NCEP reanalysis data in (top) Jan and (bottom) Jul. Contour intervals are (a) 10, (b) 10, and (c) 2.5 m s^{-1}. Easterly winds in (a) and (b) and negative values in (c) are shaded.

Two sets of perpetual January and July simulations are performed: control (CTL) simulation without the GWDC parameterization and GWDC simulation with the GWDC parameterization. For perpetual simulations, climatological monthly mean sea surface temperature and zonal-mean ozone distribution are used. The model is integrated for 3 yr in all simulations and results presented in section 4 are averages of the last 2 yr. The observational data used for comparison with the simulation results are the National Centers for Environmental Prediction (NCEP) monthly reanalysis data (R-2) for 21 yr (1979–99; Kanamitsu et al. 2002), which have a horizontal grid spacing of 2.5° latitude × 2.5° longitude and 17 vertical levels from 1000 to 10 hPa.

4. Results and discussion

a. Control (CTL) simulation

Figure 1 shows the zonal-mean zonal wind in the NCEP reanalysis data, the CTL simulation, and their differences for January and July. The zonal-mean zonal wind in the CTL simulation is reasonably acceptable in the troposphere (Hurrell et al. 1998) but is considerably different in the stratosphere compared with the NCEP reanalysis data. In the January stratosphere, underestimated westerlies at NH high latitudes, excessive easterlies in the Tropics, and excessive westerlies in the SH are observed. The underestimated westerlies in NH wintertime seem to be a unique feature of CCM3. In July, the model bias of the zonal-mean zonal wind is even larger than that in January. The polar night jet in the SH and easterlies in the tropical stratosphere are stronger than those in the NCEP reanalysis data by as much as 20 and −20 m s^{-1}, respectively. At NH high latitudes, excessive westerlies are observed both in the troposphere and stratosphere. The fact that the zonal-mean zonal wind is underestimated at NH high latitudes in wintertime where mountain drag effect is important, whereas it is overestimated in NH summertime and at SH high latitudes where mountain drag effect is small, implies that the mountain drag should not be overestimated to reduce the wind biases. This suggests a need

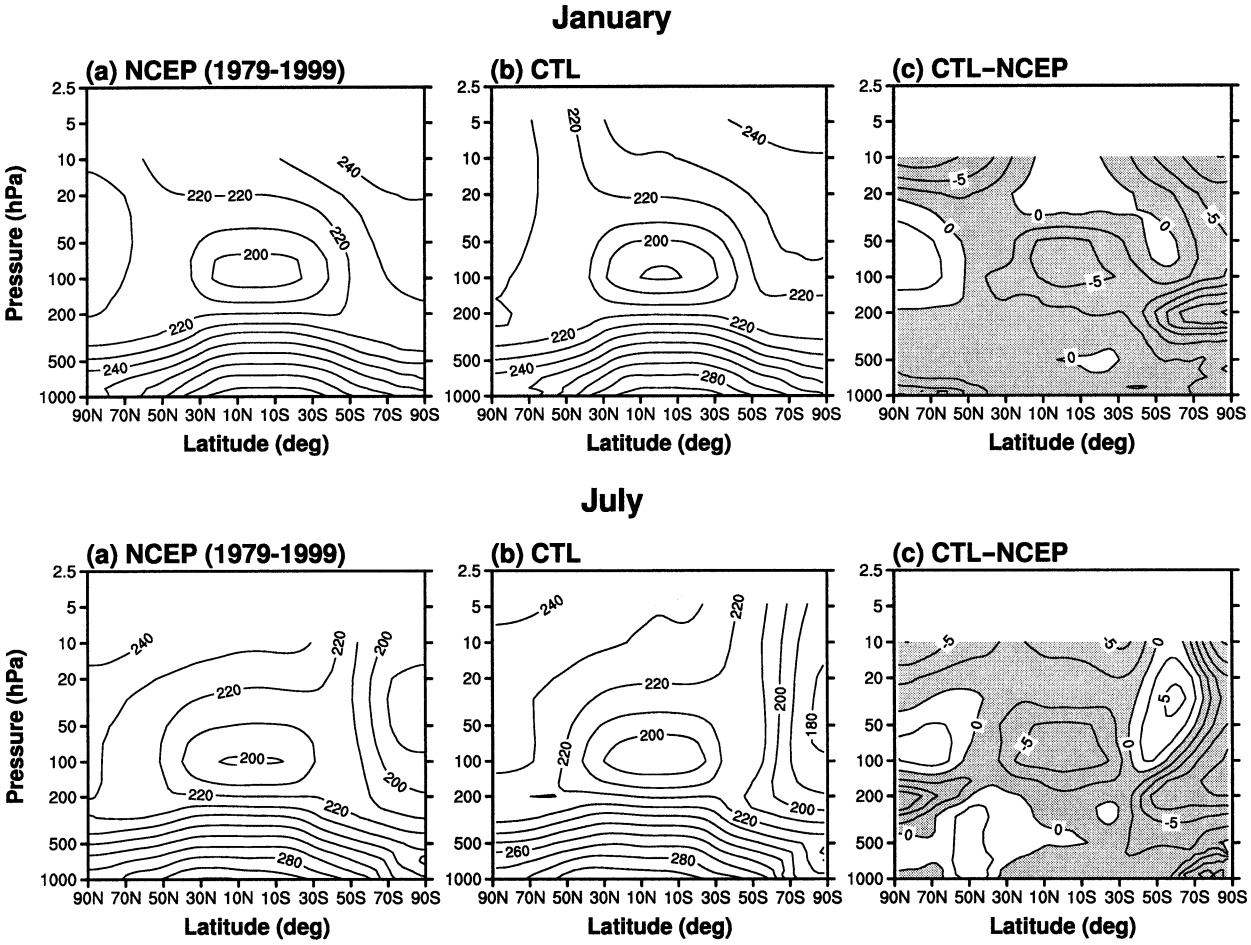

FIG. 2. The same as in Fig. 1 except for zonal-mean temperature. Contour intervals are (a) 10, (b) 10, and (c) 2.5 K. Negative values are shaded.

for a different physical process that is missing in CCM3. In addition, the fact that the low-latitude wind bias is greater in July than in January suggests that this missing process may be related to cumulus convection, which is dominant in the summer Tropics. These arguments justify the introduction of the GWDC parameterization.

In the zonal-mean temperature field (Fig. 2), significant biases are observed largely in the stratosphere and in several regions of the troposphere: cold biases at SH high latitudes and in the tropical lower stratosphere and warm biases at NH high latitudes in the lower stratosphere. The cold bias in the tropical lower stratosphere is 7 K in both January and July. The warm bias at NH high latitudes in the lower stratosphere seems to be dynamically coupled with the underestimated westerlies shown in Fig. 1, presumably due to overly strong adiabatic warming in the secondary circulation induced by mountain drag. A warm bias is also evident at NH high latitudes and SH mid- to high latitudes in the July stratosphere. Note that the magnitudes of the cold bias in the SH polar tropopause in July (~10 K) and the warm bias in the NH polar tropopause in January (~2 K) are about twice as large as those in Hack et al. (1998) obtained using 15-yr (1979–93) means of December–February and June–August CCM3 climatologies. Considering that the present results are based upon the difference between the 2-yr averaged perpetual simulation data and 21-yr averaged NCEP reanalysis data, the wind and temperature biases of the present simulations in the present study may be exaggerated. Zwiers and Boer (1987) made a systematic comparison between the perpetual and annual-cycle simulations using the Canadian Climate Centre general circulation model. They found significant differences between the perpetual and annual-cycle simulations associated with differences in radiative heating and surface balance of energy and moisture. The exaggeration of the temperature bias in the polar regions of the NH in January and SH in July in the present perpetual simulations (Fig. 2) is consistent with that of Zwiers and Boer (1987). In this study, we will not carry out detailed performance analyses of CCM3. Rather, we will emphasize the effect of the GWDC on simulated zonal-mean flow and planetary waves by

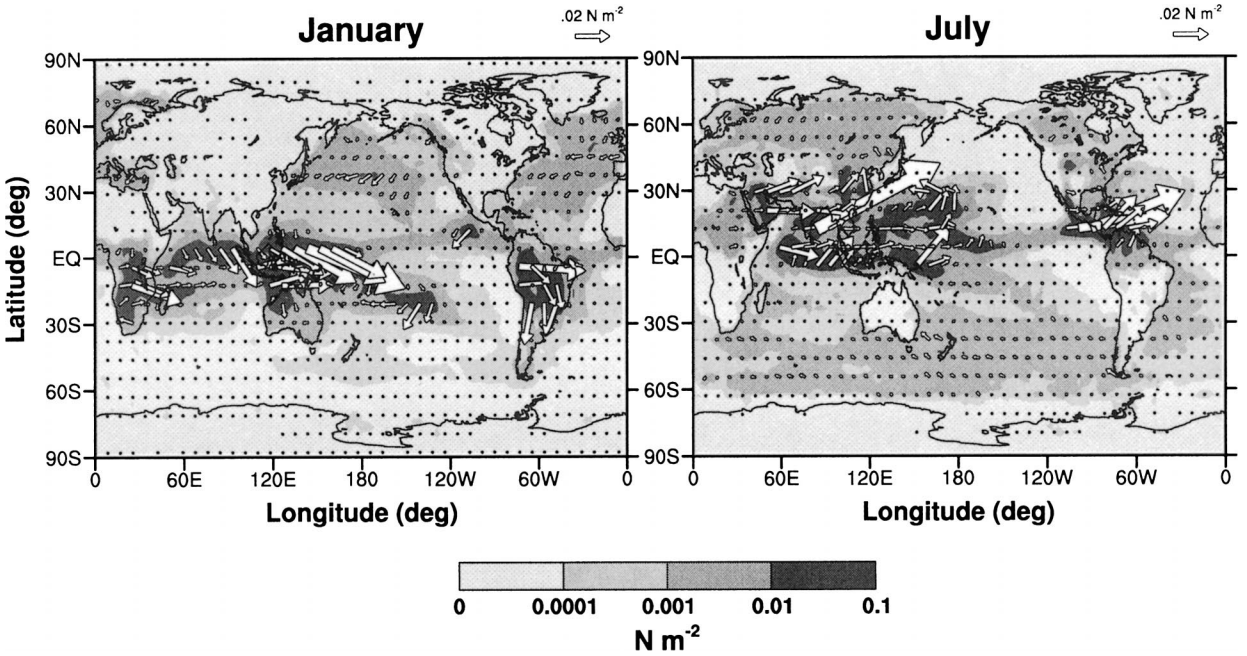

FIG. 3. Gravity wave stress vector at cloud top and its magnitude in the GWDC simulation in (left) Jan and (right) Jul.

comparing results from the CTL and GWDC simulations.

b. GWDC simulation

1) WAVE STRESS AT CLOUD TOP

Figure 3 shows the gravity wave stress vector at cloud top and its magnitude obtained from the GWDC simulation in January and July. The cloud-top wave stress is concentrated in the intertropical convergence zone (ITCZ) occupied by deep cumulus clouds. Secondary peaks are observed in the storm track regions in January and in Asia, North America, and SH midlatitude oceans in July mainly due to midlevel clouds. In major convective regions, the magnitude of gravity wave stress is in the range of 0.01–0.1 N m^{-2} with maximum values of 0.07 N m^{-2} in January and 0.1 N m^{-2} in July. The July maximum observed at just one point in the Indian Ocean is mainly due to the very small horizontal wind speed at cloud top. The magnitude range of the cloud-top wave stress (momentum flux) is comparable to that obtained from aircraft observation by Alexander and Pfister (1995; 0.12 N m^{-2}) and cloud-resolving model results by Fovell et al. (1992) and Alexander and Holton (1997) ($\sim$0.01 N m^{-2}). The radiosonde observation by Vincent and Alexander (2000) at Cocos Islands (12°S, 97°E) for a 5-yr period in the 18–25-km height range is about $\sim 7.2 \times 10^{-4}$ N m^{-2}. In the present study, the magnitude of momentum flux at the location averaged at two closest grids (12.6°S, 95.6°E and 12.6°S, 98.4°E) over 18.6–24.5-km height range is 2.2×10^{-4} N m^{-2} in January and 1.0×10^{-6} N m^{-2} in July, at least 3 times smaller than that of Vincent and Alexander. It is expected that the magnitude of the momentum flux calculated using global simulation data with a horizontal grid spacing of 2.5° latitude $\times$ 2.5° longitude and coarse vertical grid spacing in the stratosphere can be less than that observed at a single station. In general, it is not straightforward to compare the magnitudes of convectively forced gravity wave momentum fluxes obtained by various observational or numerical modeling studies. Several problems related to this issue will be discussed in section 5. The maximum magnitude of gravity wave stress in July is about half of the maximum value in Chun et al. (2001a). This is mainly because the fractional cloud coverage in the present study, which is diagnostically calculated in the model, is much less (maximum values of 0.16 in January and 0.17 in July) than the specified value of 0.4 in Chun et al. (2001a).

2) ZONAL DRAG FORCING

Figure 4 shows zonal-mean zonal wind tendency due only to the GWDC process. The zonal wind tendency is concentrated in low latitudes between 10°N and 30°S in January and 60°N and 10°S in July. In January, wave breaking occurs predominantly in the tropical lower stratosphere without any considerable amount over storm track regions where secondary peaks of cloud-top wave stress exist. In July, wave breaking occurs over relatively broader latitudes and altitudes. Strong winds in the NH midlatitude wintertime, where storm tracks are present, can rarely satisfy the wave saturation condition. The easterly acceleration below the westerly ac-

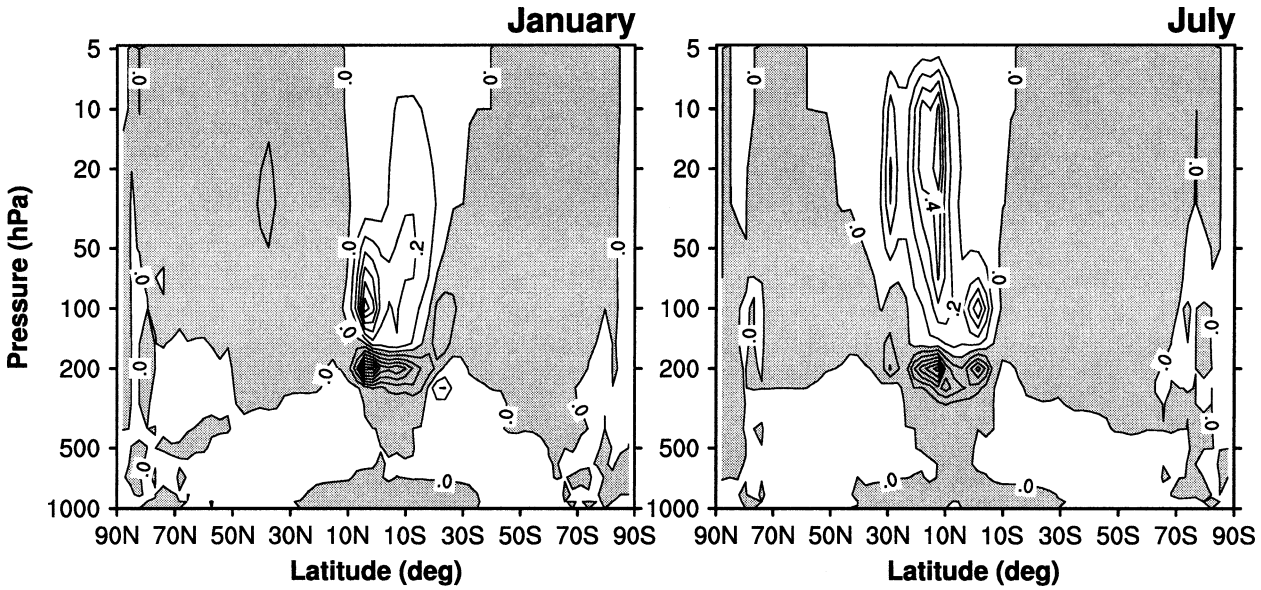

FIG. 4. Zonal-mean zonal wind tendency due to the GWDC parameterization in (left) Jan and (right) Jul. Contour interval is 0.1 m s^{-1} day^{-1} and negative values are shaded.

celeration (Fig. 4) is the compensating acceleration for the momentum closure. Since the prevailing zonal-mean zonal wind is easterly in the tropical region, the zonal-mean zonal wind is decelerated by the GWDC process in the stratosphere but accelerated in the troposphere just below cloud top. Maximum values of westerly acceleration above cloud top and easterly acceleration below it are 0.66 and -0.74 m s^{-1} day^{-1} in January and 0.58 and -0.64 m s^{-1} day^{-1} in July. Since the downward momentum flux by gravity waves from cloud top to model top is assumed to be deposited into just one layer below cloud top, following a numerical study by Kershaw (1995), the maximum magnitude of the easterly acceleration is larger than that of westerly acceleration. The magnitude of the easterly acceleration in the cloud region can depend on the method of redistributing the momentum into the cloud region. However, given that the air density increases going downward, acceleration by momentum deposition in the cloud region is predominant in the upper cloud region, even with an evenly distributed momentum deposition throughout the entire cloud region. In reality, momentum flux in the cloud region is mainly accomplished by cloud momentum flux due to turbulence rather than by gravity waves, as suggested to be parameterized in large-scale models by Wu and Moncrieff (1996) and Gregory et al. (1997). In order to complete momentum conservation for an entire air column, cloud momentum in the cloud region and gravity wave momentum above cloud top should be considered together. When these two processes are coupled, some adjustment may be needed near cloud top.

Figure 5 shows the vertical profile of zonal wind tendency due to the GWDC parameterization averaged over 5°N–5°S, together with the zonal-mean zonal wind. The positive zonal drag forcing above cloud top is concentrated in the layer of 150–30 hPa in January and is confined below 70 hPa in July. Maximum westerly acceleration is 0.41 m s^{-1} day^{-1} (0.32 m s^{-1} day^{-1}) at 100 hPa and maximum easterly acceleration is -0.59 m s^{-1} day^{-1} (-0.28 m s^{-1} day^{-1}) at 200 hPa in January (July). The maximum magnitude of easterly acceleration is larger in January because wave breaking occurs over a deeper layer, so that vertically integrated westerly momentum from cloud top to model top is larger in January. The relatively weak zonal wind above cloud top between 150 and 30 hPa in January provides a favorable condition for wave breaking. In CB98, the saturated zonal momentum flux is given by $\tau_s = -[\rho U^3/(N\Delta x)]c_1 c_2^2 \mu_s^2$, where U is the horizontal wind at a certain height above cloud top in the direction of the cloud-top wave stress vector and μ_s is the nonlinearity factor for saturation of thermally induced internal gravity waves. At 70 hPa, the calculated wave stress averaged over 5°N–5°S is 8 $\times 10^{-4}$ N m^{-2} in January and 5 $\times 10^{-4}$ N m^{-2} in July. The wave can be saturated when U is less than about 3.5 m s^{-1} and 3.0 m s^{-1} in January and July, respectively, with $N = 0.025$ s^{-1}, $\rho = 0.12$ kg m^{-3}, $\Delta x =$ 250 km, and $\mu_s = 2.2$. Since the magnitude of zonal-mean zonal wind at 70 hPa is 0.86 m s^{-1} in January and 3.3 m s^{-1} in July, wave breaking occurs in January. This result implies that the magnitude and location of gravity wave drag strongly depend not only on the magnitude and location of wave sources but also on the wave propagation conditions in terms of the vertical profiles of wind and stability.

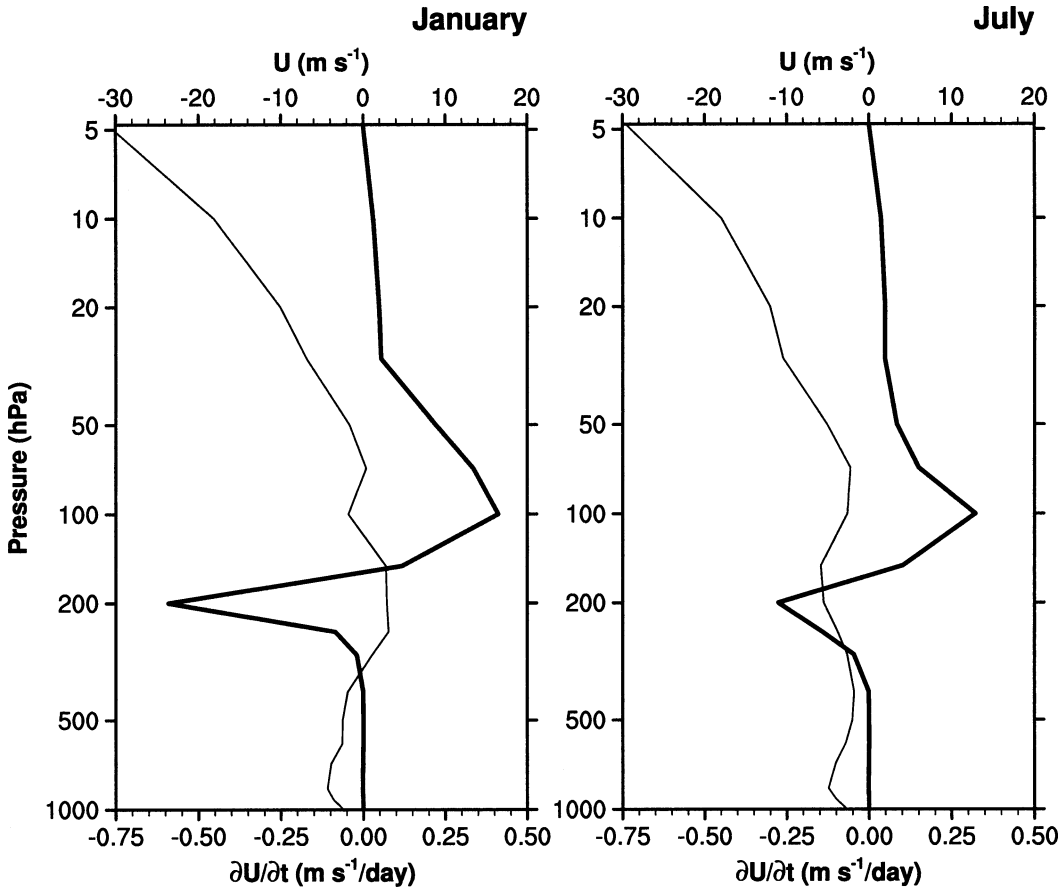

FIG. 5. Vertical profiles of zonal-mean zonal wind (thin line) and zonal wind tendency (thick line) due to the GWDC parameterization averaged over 5°N–5°S in (left) Jan and (right) Jul.

3) ZONAL-MEAN ZONAL WIND AND TEMPERATURE

In order to examine the effect of the GWDC parameterization on the CCM3-simulated climate, the differences in zonal-mean zonal wind and temperature between the CTL simulation and NCEP reanalysis data (CTL − NCEP) and the GWDC and CTL (GWDC − CTL) simulations are plotted in Fig. 6. In both January and July, the maximum impact of the GWDC parameterization occurs in the tropical stratosphere between 30°N and 30°S, where excessive easterlies appear in the CTL simulation compared with the NCEP reanalysis data (Fig. 6a). It is clear that including the GWDC parameterization significantly alleviates the zonal-mean zonal wind bias of CCM3 in the tropical stratosphere. At 0°N, 30 hPa (25°N, 10 hPa), where the maximum easterly bias exists in January (July), the GWDC process reduces model bias by as much as 59% (40%). At locations where the maximum impact of the GWDC parameterization occurs (GWDC − CTL), model bias (CTL − NCEP) is reduced by more than 50%. The GWDC process also alleviates the excessive westerly bias in the tropical upper troposphere. The locations of model bias and GWDC impact are reasonably well matched in the Tropics. In the extratropical regions, the GWDC impact on zonal-mean zonal wind is small but including the GWDC parameterization generally reduces model error.

The impact of the GWDC parameterization on zonal-mean temperature (Fig. 6b) is prominent in the tropical lower stratosphere where a cold bias exists in the CTL simulation (Fig. 2). The cold bias in the tropical lower stratosphere is reduced with the GWDC parameterization by as much as 44% in January (0°, 70 hPa) and 32% in July (0°, 70 hPa). It is noteworthy, however, that the percentage change of model bias in the zonal-mean zonal wind and temperature fields by including the GWDC parameterization might not be very reliable because the bias of the CTL simulation compared with the NCEP reanalysis data can be either exaggerated or underrated in the present study due to the different averaging periods used in the two datasets. The impact of the GWDC parameterization on zonal-mean temperature is relatively small compared with its impact on zonal-mean wind. This is because the temperature change by the GWDC process is through a secondary circulation induced by drag forcing, while the zonal wind change

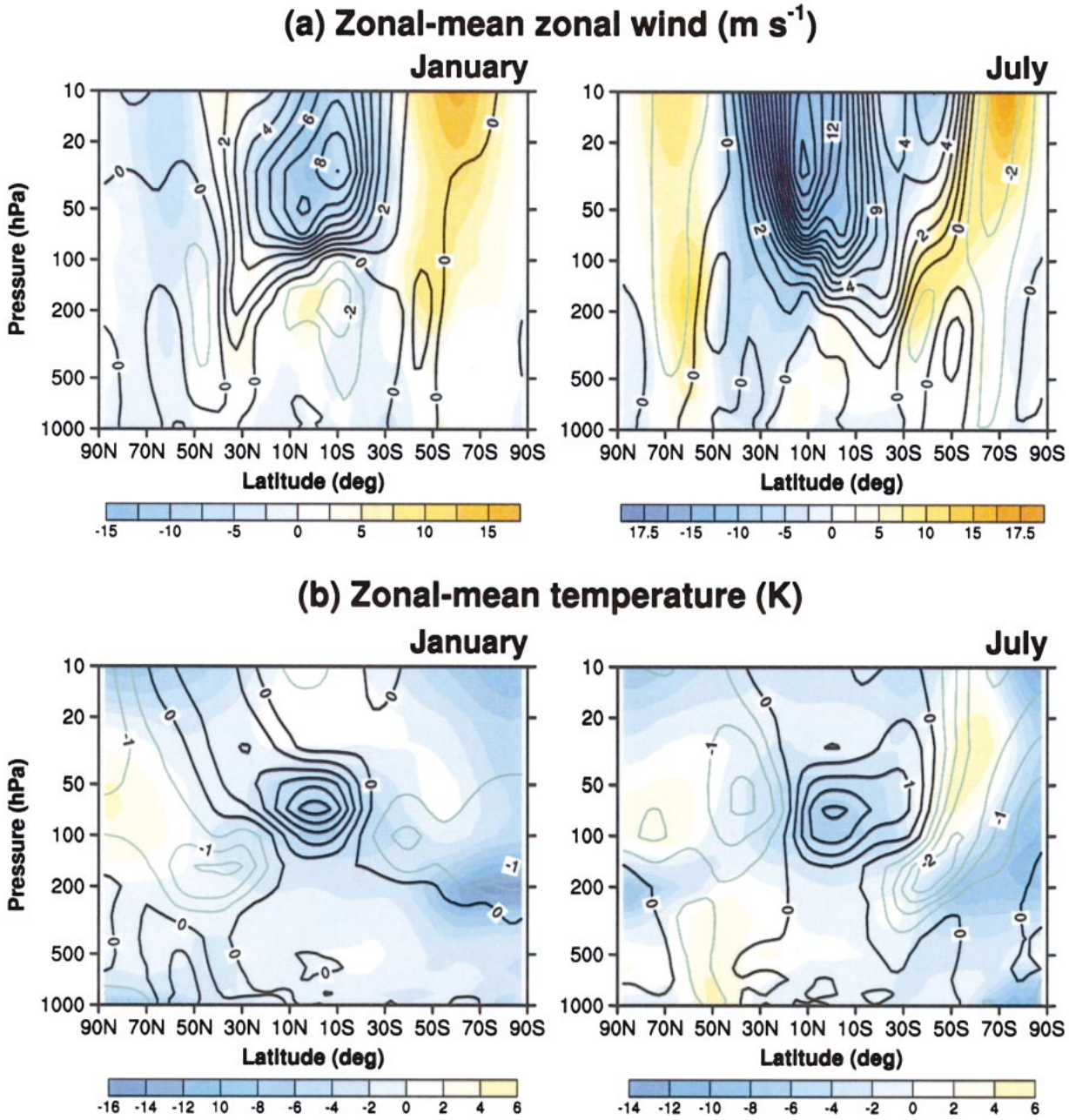

FIG. 6. Differences in zonal-mean (a) zonal wind and (b) temperature between the CTL simulation and NCEP reanalysis data (CTL − NCEP) shown in color shading and the GWDC and CTL simulations (GWDC − CTL) shown in contours in (left) Jan and (right) Jul. Contour intervals are (a) 1 m s^{-1} and (b) 0.5 K.

is due directly to drag forcing. A schematic of the secondary circulation induced by the positive drag forcing above cloud top and the negative drag forcing just below it in the ITCZ, which appears in Fig. 4, is drawn in Fig. 7. The ITCZ is ideally assumed to be shifted in the NH and SH. This zonal drag pattern produces northerly (southerly) flow above cloud top and southerly (northerly) flow below it in the NH (SH). The downward branch is located near the equator regardless of ITCZ location. The adiabatic warming in the downward branch of the secondary circulation is responsible for warming in the tropical lower stratosphere centered near the equator in both January and July, as shown in Fig. 6b.

4) HORIZONTAL WIND DIVERGENCE IN THE TROPICS

Figure 6 demonstrates that the zonal-mean zonal wind and temperature fields of CCM3 are significantly im-

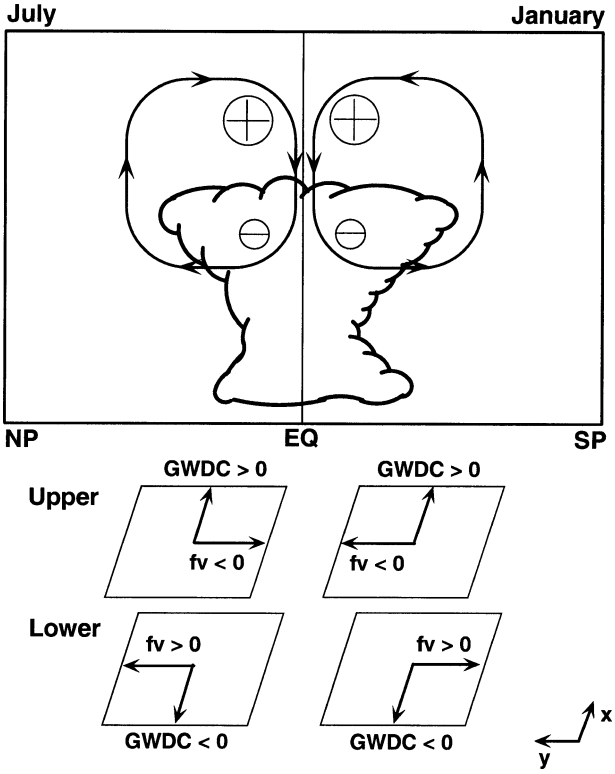

FIG. 7. A schematic of the secondary circulation induced by positive drag forcing above cloud top and negative drag forcing below it in ITCZ that are ideally assumed to be located in the SH and NH. The lower part shows zonal drag force and induced Coriolis force in a horizontal plane above and below cloud top. The plus and minus indicate signs of zonal drag forcing by convective gravity waves.

proved in the tropical region from the upper troposphere to the stratosphere by including the GWDC parameterization. The effect of the GWDC parameterization on the tropical circulation can be clearly seen in the horizontal wind divergence at 100 hPa in the CTL simulation, the difference between the CTL simulation and NCEP reanalysis data (CTL − NCEP), and the difference between the GWDC and CTL simulations (GWDC − CTL) in January (Fig. 8) and July (Fig. 9). In January, the CTL simulation exhibits strong divergence in the western Pacific, where major convective activity exists, and strong convergence in surrounding area. A dipole-like pattern of strong divergence and convergence in the central Pacific is also evident. The magnitude of model bias (CTL − NCEP) is comparable to that of the CTL simulation itself. Including the GWDC parameterization (GWDC − CTL) significantly reduces the excessive divergence and convergence bias in the major convective regions. Improvement of CCM3 performance in the horizontal wind divergence field by including the GWDC parameterization is more clearly seen in July (Fig. 9). The excessive convergence and divergence bias near the Indian Ocean, where major convective activity exists in July, is almost completely alleviated by the GWDC process.

The accurate simulation of horizontal wind divergence/convergence near cloud top is expected to lead to a more realistic pattern of horizontal wind divergence/convergence in the lower troposphere. However, the difference in horizontal wind divergence at 850 hPa between the GWDC and CTL simulations (not shown) is very small. Especially in July, almost no change is found in the tropical region between 30°N and 30°S. This indicates that the effect of the GWDC parameterization is confined between the upper troposphere and stratosphere without any significant impact on the lower troposphere. This is because wave drag forcing is imposed from one level below cloud top, which generally reaches the tropopause in the tropical region, to the model top. Also, the secondary circulation induced by drag forcing (Fig. 7) is highly localized above the upper troposphere.

c. Effect on planetary waves

1) WAVE AMPLITUDE

Momentum forcing by the GWD parameterization, whether its source is mountain or convection, can generate planetary waves as a source of potential vorticity (Pierrehumbert 1986; Andrews et al. 1987) and modify the amplitude and phase of planetary waves through the change of zonal-mean flow. Figure 10 shows the difference in the zonal-mean amplitude of geopotential height perturbation between the GWDC and CTL simulations for stationary zonal wavenumbers 1 to 3 in January and July. The impact of the GWDC process on planetary waves in the stratosphere is predominant in the winter hemisphere (especially in July) and its impact in the troposphere is comparable in both the summer and winter hemispheres (especially for wavenumbers 2 and 3 in January). In the stratosphere, the amplitude of wavenumber 1 increases slightly in NH midlatitudes in January and decreases significantly in the SH mid-to-high latitudes in July. Compared with the NCEP reanalysis data at 10 hPa (Fig. 11), the excessive amplitude of wavenumber 1 in the July SH that appeared in the CTL simulation is reduced significantly by including the GWDC parameterization. In the January NH, the increased amplitude of wavenumber 1 is negligibly small compared with model bias. The amplitude of wavenumber 2 increases mainly at SH high latitudes in July, thus improving model performance significantly (Fig. 11). On the other hand, the amplitude of wavenumber 3 increases (decreases) at NH (SH) mid-to-high latitudes in January (July), which reduces (amplifies) model bias slightly. In Fig. 11, the amplitudes of planetary waves in the CTL and GWDC simulations and the NCEP reanalysis data are compared at a single level of 10 hPa. As shown in Fig. 10, however, the impact of the GWDC parameterization on planetary waves varies with height. Hence, the result in Fig. 11 may not be directly applicable to other levels. In the stratosphere (above ~100 hPa), the impact of the GWDC parame-

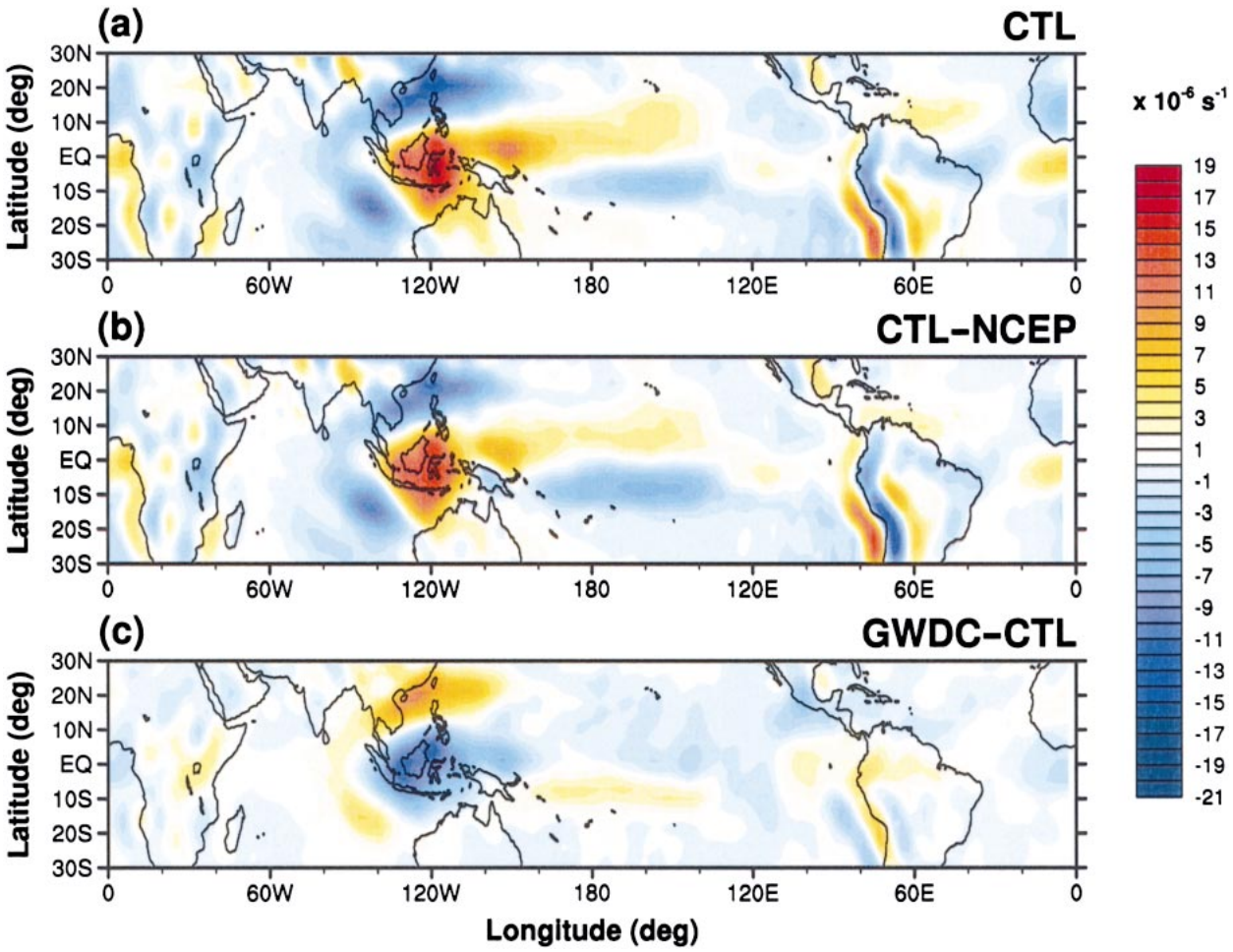

FIG. 8. Horizontal wind divergence at 100 hPa in the tropical area (30°N–30°S) in Jan: (a) CTL simulation, (b) difference between the CTL simulation and NCEP reanalysis data (CTL − NCEP), and (c) difference between the GWDC and CTL simulations (GWDC − CTL).

terization on planetary waves and the comparison results with the NCEP reanalysis data are found to be qualitatively similar to those in Fig. 11, while they are different in the troposphere.

The preceding results are somewhat different from those of Chun et al. (2001a) who considered the impact of the GWDC parameterization in YONU GCM on planetary waves of zonal wavenumbers 1 and 2 in July. In Chun et al. (2001a), the amplitude of wavenumber 1 increases at both NH and SH high latitudes (inconsistent with the current study) and the amplitude of wavenumber 2 increases exclusively in the SH (consistent with the current study). Both the increased amplitudes of wavenumbers 1 and 2 in the SH improved the performance of YONU GCM (see Fig. 11 of Chun et al. 2001a). It is interesting that even though the impact of the GWDC parameterization on the amplitude of wavenumber 1 in SH wintertime in CCM3 is different from that in YONU GCM, both models are improved by including the GWDC parameterization. Considering that the amplitude change of planetary waves by the GWDC forcing is through a more subtle nonlinear process than the change of zonal-mean flow, improvement of model performance in planetary waves regardless of the characteristics of each model implies that the GWDC parameterization is an important physical process that should be included in GCMs.

2) ELIASSEN–PALM FLUX DIVERGENCE

The forcing by planetary waves on zonal-mean zonal wind can be best expressed by Eliassen–Palm (EP) flux divergence forcing (Andrews et al. 1987):

$$\frac{1}{\rho_0 a\cos\phi}\nabla\cdot\mathbf{F}=\frac{1}{\rho_0 a\cos\phi}\left[\frac{1}{a\cos\phi}\frac{\partial}{\partial\phi}(F_\phi\cos\phi)+\frac{\partial F_z}{\partial z}\right], \tag{3}$$

where

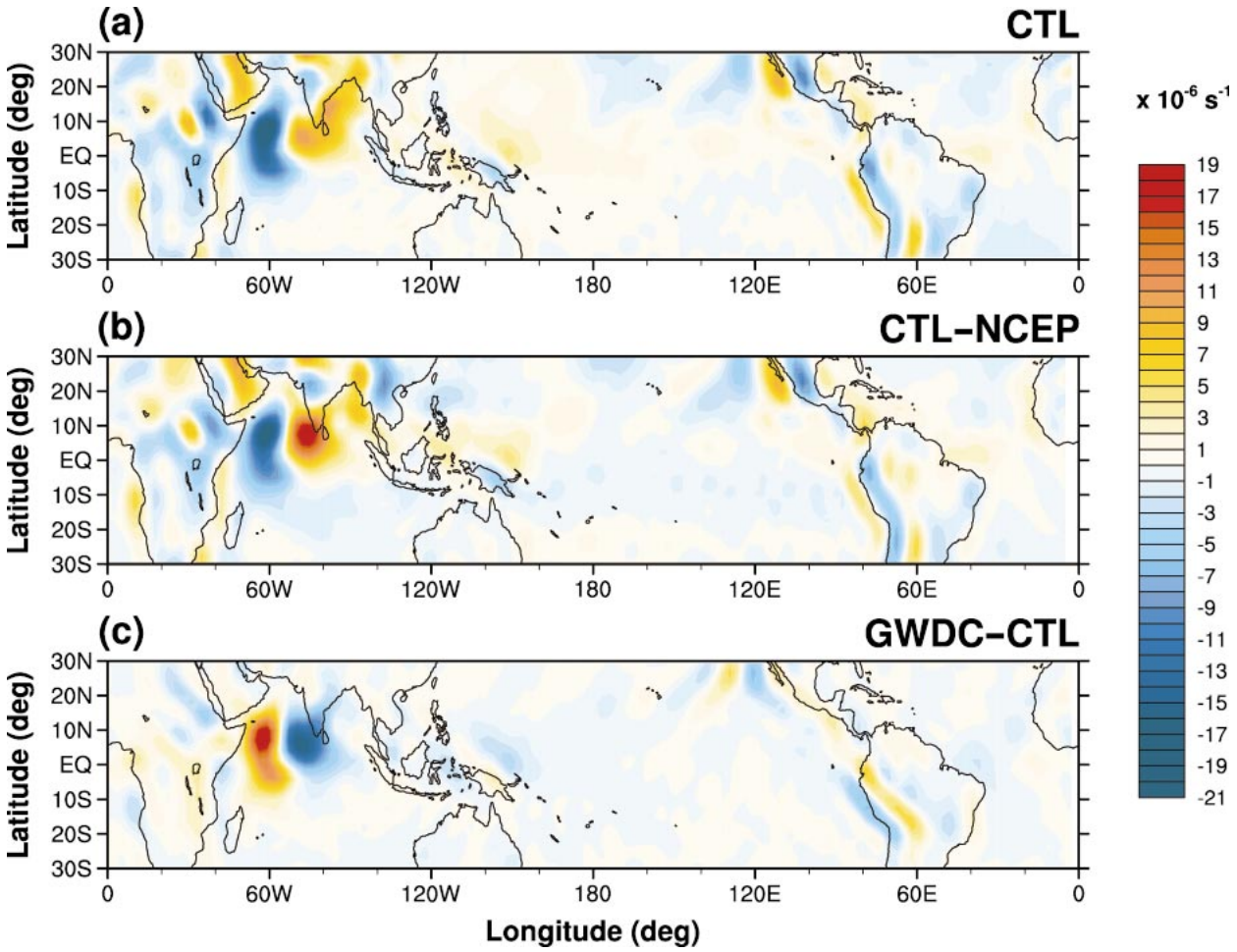

FIG. 9. The same as in Fig. 8 except for Jul.

$$F_\phi = \rho_0 a \cos\phi \left(\frac{\partial \overline{u}}{\partial z} \frac{\overline{v'\theta'}}{\partial \overline{\theta}/\partial z} - \overline{v'u'} \right),$$

$$F_z = \rho_0 a \cos\phi \left\{ \left[f - \frac{1}{a\cos\phi} \frac{\partial}{\partial \phi} (\overline{u}\cos\phi) \right] \frac{\overline{v'\theta'}}{\partial \overline{\theta}/\partial z} - \overline{w'u'} \right\}.$$

Here, θ is the potential temperature, u, v, and w are the zonal, meridional, and vertical components of wind, respectively, and z is the log pressure height [$z \equiv -H \ln(p/p_s)$, where H is the scale height assumed to be 7 km, p is the pressure, and $p_s = 1000$ hPa], ρ_0 is the basic-state density [$\rho_0 = \rho_s \exp(-z/H)$], a is the radius of the earth, ϕ is the latitude, and f is the Coriolis parameter. The overbar means the zonal mean and the prime the departure from zonal-mean value.

Figure 12 shows the differences in the EP flux vector and its divergence forcing between the GWDC and CTL simulations in the January and July stratosphere by stationary and transient waves. Transient waves are the deviation of geopotential height perturbation from its 2-yr averaged value. The impact of the GWDC parameterization on EP flux forcing is predominant in winter hemisphere mid- to high latitudes. By contrast, the magnitude is minimal in the tropical stratosphere where the zonal-mean zonal wind difference between the GWDC and CTL simulations is maximal (Fig. 6a). The impact of the GWDC process on EP flux divergence forcing is stronger in the NH than in the SH, even though the amplitude change of stationary waves by the GWDC process is larger in the July SH (Fig. 10). In the NH wintertime, the effect of the GWDC on EP flux divergence by stationary waves is opposite to that by transient waves above $z = 25$ km. Because of this opposing effect, the zonal-mean zonal wind change due to the GWDC parameterization is very small at mid-to-high latitudes in the January stratosphere (Fig. 6a). The GWDC process enhances the downward component of EP flux at latitudes poleward of about 60°N for both stationary and transient waves. In the tropical region between 30°N and 30°S, EP flux divergence by transient waves is negligibly smaller than that by stationary waves. EP flux vectors due to stationary waves are directed equatorward from 30°N and downward near 20°S below $z =$ 20 km. In the July SH, EP flux is directed downward

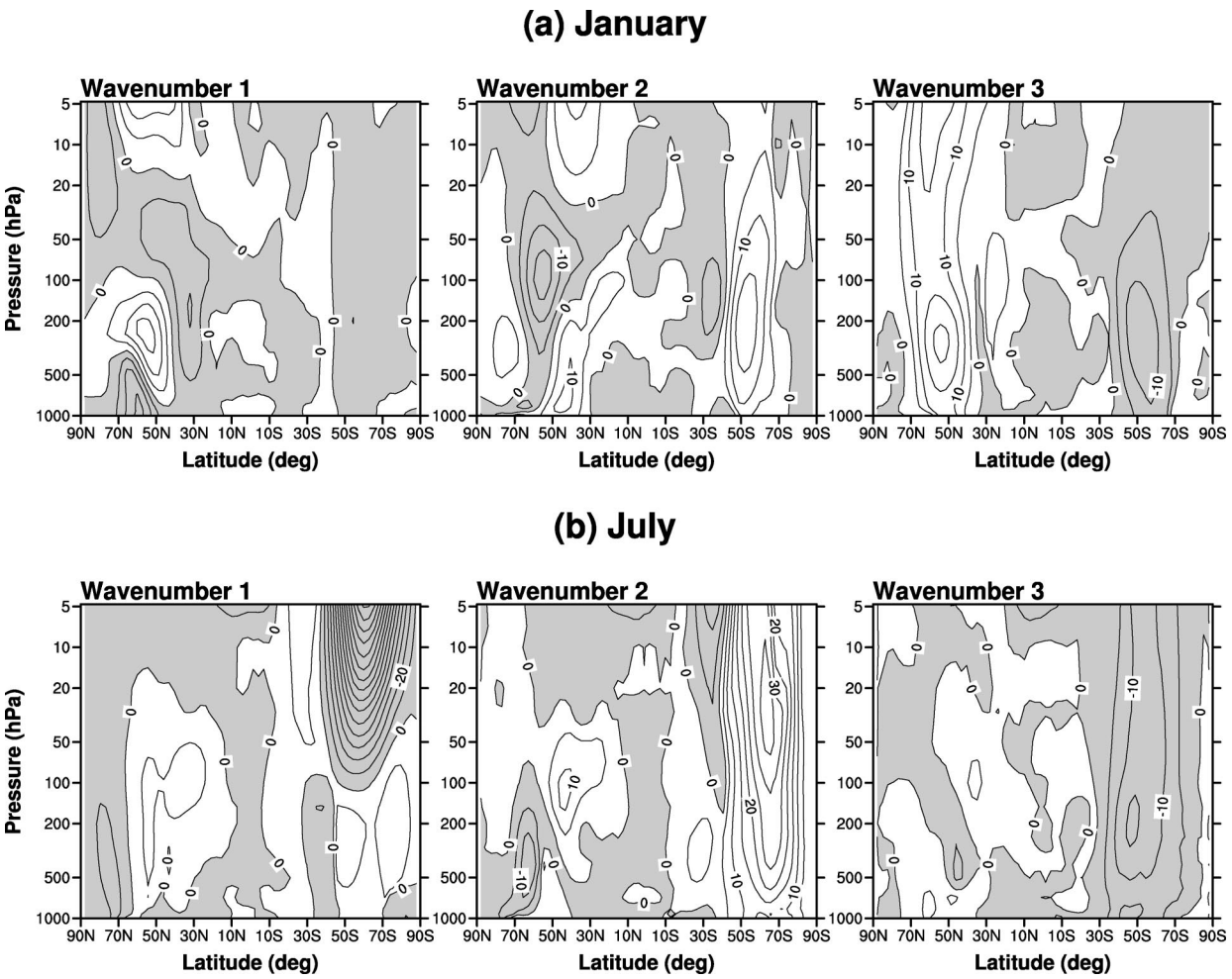

FIG. 10. Latitude–height cross section of difference in the wave amplitude of geopotential height perturbation between the GWDC and CTL simulations (GWDC − CTL) for zonal wavenumbers 1–3 in (a) Jan and (b) Jul. Contour intervals for wavenumbers 1–3 are 10, 5, and 5 m, respectively.

and poleward by stationary waves and upward and equatorward by transient waves from about 40°S above $z = 20$ km. Since EP flux divergence forcing by stationary and transient waves are not opposite to each other, the zonal-mean zonal wind change by the GWDC process at mid-to-high latitudes in the stratosphere is relatively large in the July SH (westerly acceleration between 30° and 50°S and easterly acceleration poleward from 50°S above $z = 20$ km) than in the January NH, as shown in Fig. 6a. The difference in EP flux divergence forcing between the GWDC and CTL simulations is, however, very small compared to the model bias.

Figure 13 shows EP flux divergence forcing at 10 hPa in the CTL and GWDC simulations and in the NCEP reanalysis data for stationary waves and United Kingdom Met Office (UKMO) daily assimilation data (Swinbank and O'Neill 1994) for 7 yr (1993–99) for transient waves. In NH wintertime, simulated EP-flux divergence forcing is 2–3 times smaller than the observed, while it is reasonably comparable in the SH and tropical region in January and at all latitudes in July except at SH mid-to-high latitudes. This result implies that the impact of the GWDC on planetary waves through nonlinear processes is rather small and that the zonal-mean zonal wind change is mainly due to the direct drag forcing and induced secondary circulation (Fig. 7), which are mainly confined in the tropical region.

d. Effect on QBO

In the current perpetual January and July simulations, interannual variations of zonal-mean zonal wind cannot be simulated. However, since the zonal-mean zonal wind and temperature are significantly improved in the tropical stratosphere by including the GWDC parameterization, one is tempted to examine the impact of the GWDC on the QBO based upon the present results. The zonal drag forcing by the GWDC parameterization averaged over 5°N–5°S (Fig. 5) in January shows a maximum value of 0.41 m s^{-1} day^{-1} near 100 hPa and de-

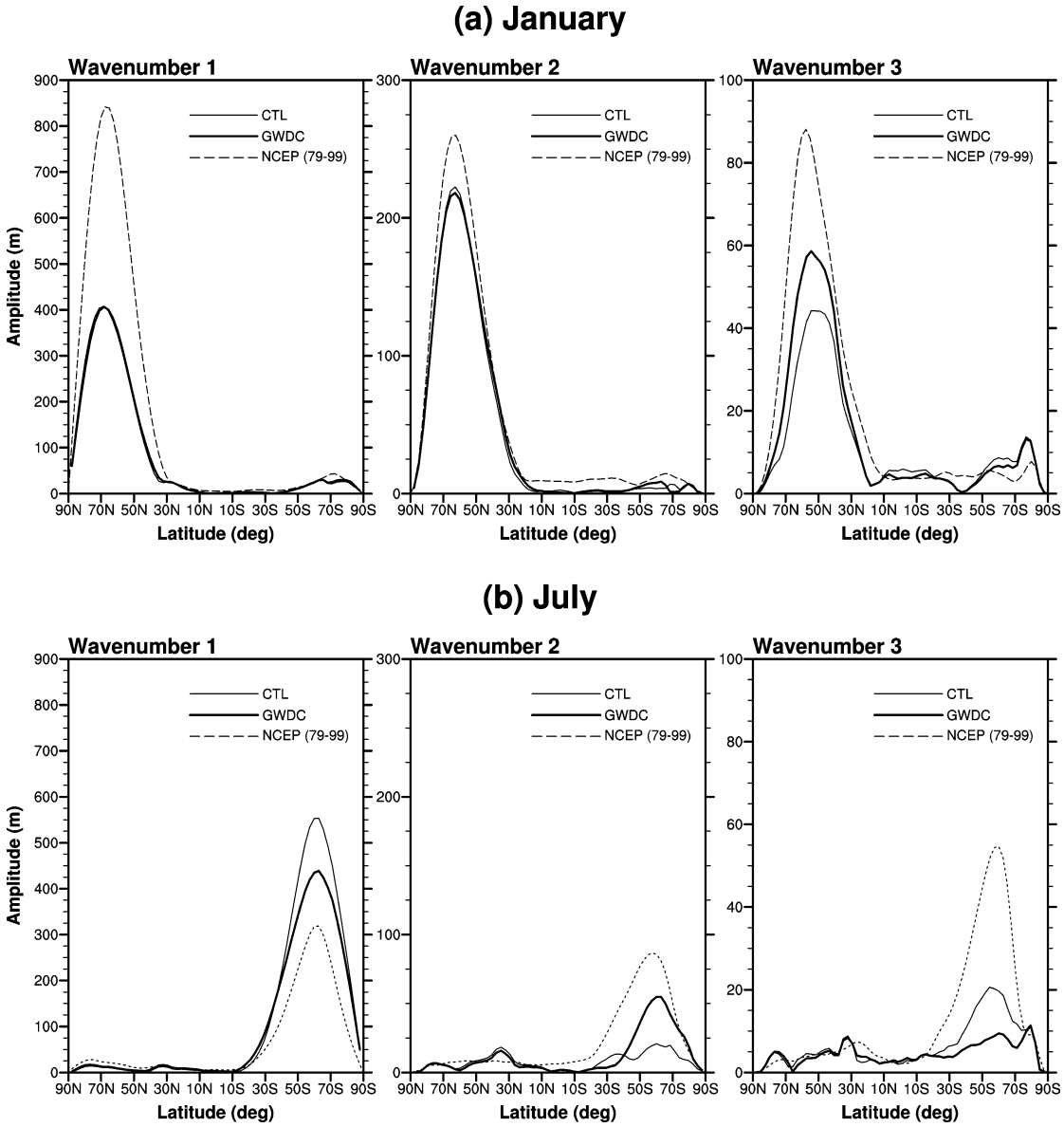

FIG. 11. Amplitude of geopotential height perturbation for zonal wavenumbers 1–3 at 10 hPa in the CTL simulation (thin solid line), GWDC simulation (thick solid line), and NCEP reanalysis data (dashed line) in (a) Jan and (b) Jul.

creases with height, with its values of 0.05 m s^{-1} day^{-1} and a zonal-mean zonal wind of -6.9 m s^{-1} at 30 hPa. In July, the zonal drag forcing at 30 hPa is 0.05 m s^{-1} day^{-1} and the zonal-mean zonal wind is -10.4 m s^{-1}. When the zonal-mean zonal wind at 30 hPa is compared with the composite latitude–time cross section of zonal-mean zonal wind by Dunkerton and Delisi (1985, their Fig. 17) that was obtained from radiosonde observations for 18 yr, the present case is roughly matched to about one month before the zonal wind change from easterly to westerly. At this time, the observed zonal drag forcing at 30 hPa is about 10 m s^{-1} $month^{-1}$ ($\sim$0.33 m s^{-1} day^{-1}) around $\pm 5°$ latitudes. This implies that the zonal drag forcing due to breaking stationary convective gravity waves in the GWDC simulation can explain about 15% of that required to drive the westerly QBO phase.

For an investigation of the effect of the GWDC parameterization on the QBO, a longer integration allowing interannual variations of boundary conditions is required. Recently, Scaife et al. (2002) successfully showed that including a spectral gravity wave drag parameterization based upon a parameterization scheme by Warner and McIntyre (1999) can reproduce the QBO in the Met Office Unified Model. Even though interannual variations of boundary conditions are not allowed and the imposed wave forcing is constant in time and space, their simulated zonal-mean zonal wind reasonably resembles the observed QBO. One of the lim-

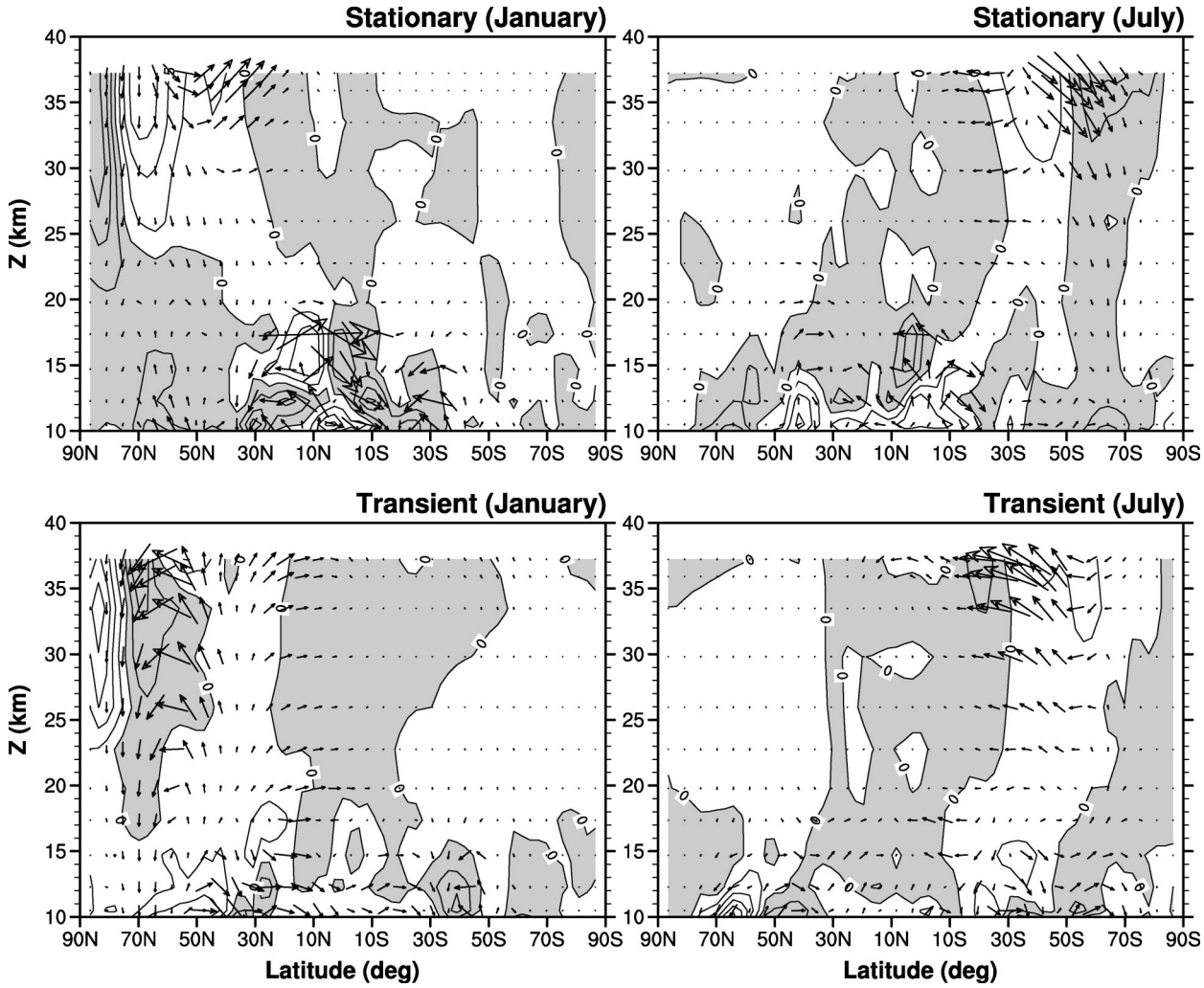

FIG. 12. Latitude–height cross section of difference in EP flux vector and its divergence forcing between the GWDC and CTL simulations (GWDC − CTL) in (left) Jan and (right) Jul by (top) stationary and (bottom) transient waves. Contour interval is 0.25 m s^{-1} day^{-1} and negative values are shaded.

itations of the current parameterization is that the gravity waves considered are stationary relative to the ground. Gravity waves considered in the GWDC parameterization by CB98 are stationary relative to a moving convective source, but they are effectively stationary relative to the ground in GCMs because cloud movement cannot be accounted for in current cumulus parameterization schemes. Thus, the impact of the GWDC on zonal-mean flow is mainly in the tropical lower stratosphere where the zonal-mean zonal wind is small enough for breaking stationary waves. However, if the zonal wind varies seasonally and interannually, wave breaking can occur at higher altitudes. Using the data of 10-yr (1979–88) integration of YONU GCM with boundary conditions provided by AMIP (Atmospheric Model Intercomparison Project; Gates 1992), Chun et al. (2001b) showed that seasonal and interannual variations of cloud-top wave stress and wave drag are strongly dependent upon those of wind, temperature, and convective activity. The impact of the GWDC on interannual variations of CCM3-simulated climate associated with the QBO remains to be done in the future by extending the parameterization of CB98 by including nonstationary waves. It is noteworthy that the vertical resolution of the model is another important factor for reproducing QBO-like oscillations in GCMs. The models that could succeed to reproduce QBO-like signals (e.g., Hamilton et al. 1999; Scaife et al. 2002; Giorgetta et al. 2002) have much higher vertical resolution than the CCM3 used in this study.

5. Discussion, summary, and conclusions

The parameterization of convectively forced internal gravity waves proposed by Chun and Baik (1998) was implemented into NCAR CCM3 and the effect of grav-

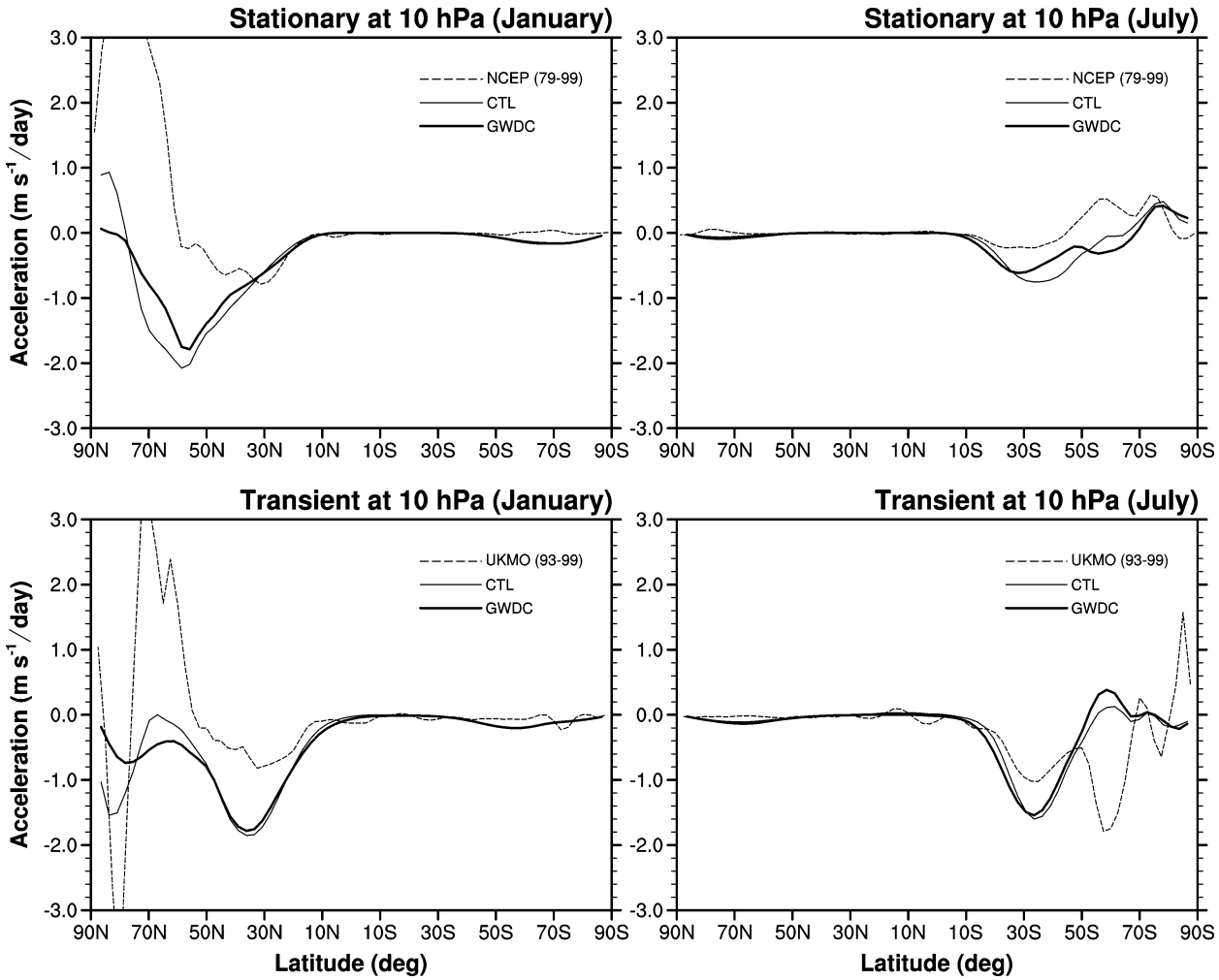

FIG. 13. Eliassen–Palm flux divergence forcing at 10 hPa in the CTL and GWDC simulations and in the NCEP reanalysis data for stationary waves and UKMO assimilation data for transient waves.

ity wave drag induced by cumulus convection (GWDC) on the atmosphere general circulation was investigated through perpetual January and July simulations. It was shown that the cloud-top wave stress is concentrated in the intertropical convergence zone where major convective activity exists and that its magnitude is reasonably comparable to observations and cloud-resolving modeling results considering the horizontal and vertical resolutions of CCM3. The zonal drag forcing by the GWDC process is largely confined in the tropical lower stratosphere with westerly acceleration above cloud top and easterly acceleration just below it. Wave breaking occurs in the tropical lower stratosphere where the zonal wind is very weak. This is because gravity waves considered in the present parameterization are stationary relative to the ground under the cumulus parameterization used in CCM3.

The impact of the GWDC parameterization on zonal-mean zonal wind and temperature was that the GWDC parameterization significantly alleviates systematic model biases. In particular, excessive easterlies in the tropical stratosphere and excessive cold temperatures in the tropical lower stratosphere are significantly alleviated. The temperature change is mainly due to the secondary circulation induced by drag forcing. A dipole of positive drag forcing above cloud top and negative drag forcing just below it produces a downward branch near the equator and the resultant adiabatic warming is responsible for alleviating the cold bias that appeared in the tropical lower stratosphere. The impact of the GWDC parameterization on the tropical atmosphere was clearly shown in the horizontal wind divergence at 100 hPa. The excessive divergence and convergence pattern in the western Pacific in January and the Indian Ocean in July where major convective activity exists is significantly improved by including the GWDC parameterization. However, the effect of the GWDC on the horizontal wind divergence is localized above the upper troposphere and no comparable impact is found in the lower troposphere.

The effect of the GWDC parameterization on planetary waves was studied by examining the amplitudes of zonal wavenumbers 1–3 and EP flux divergence forcing by stationary and transient waves. The amplitude change due to the GWDC process is mainly in the winter hemisphere and stronger impacts occur in the July SH where the decreased amplitude of wavenumber 1 and the increased amplitude of wavenumber 2 improve model performance in the stratosphere. In January, the amplitude change by the GWDC process is negligibly small compared with model bias except for wavenumber 3 that improves model performance notably. The impact of the GWDC parameterization on EP flux divergence forcing by stationary and transient waves is predominant at winter hemisphere mid-to-high latitudes and its impact by stationary waves is opposite to that by transient waves. Consequently, the zonal-mean zonal wind change by the GWDC process is mainly due to the direct drag forcing in the tropical region without any considerable contribution by planetary waves in the extratropics through nonlinear process. This result differs from that found in Chun et al. (2001a) who showed that the zonal-mean zonal wind change by the GWDC parameterization in YONU GCM is dominant in the SH mid-to-high latitudes in the perpetual July simulation through the nonlinear processes in terms of planetary waves. It is not straightforward to understand the difference because the two models have different physical processes as well as model configuration. CCM3 has finer horizontal and vertical resolutions and the zonal-mean zonal wind and temperature fields simulated using CCM3 (Figs. 1 and 2) are more realistic than those simulated using YONU GCM (Fig. 1 of Chun et al. 2001a).

The present GWDC parameterization can provide a global distribution of wave momentum flux at source level (cloud-top height), which is self-consistently calculated in a numerical model with wind, temperature, air density, and convective heating information. This is one of the merits for the first-type GWD parameterization schemes mentioned in the introduction, compared with the wave spectrum method in which the spatial and temporal variations of wave momentum flux at the source level cannot be internally calculated but must be specified a priori. In the present parameterization, the global distribution of wave momentum flux at source level is largely determined by the global distribution of convective clouds so that an accurate representation of subgrid-scale cumulus convection is required. Ricciardulli and Garcia (2000) calculated the convective heating rate in CCM3 using two cumulus parameterization schemes (Hack 1994; Zhang and McFarlane 1995) and compared the model results with those estimated using satellite-produced brightness temperature in the tropical region. They showed that the variability of convective activity and the resultant wave momentum flux induced by convective forcing is severely underestimated in the model, especially with the Zhang and McFarlane scheme. A recent study by Horinouchi (2002), however, showed that Ricciardulli and Garcia's estimation of convective precipitation is too strong compared with radar-derived precipitation during the Tropical Ocean Global Atmosphere Coupled Ocean–Atmosphere Response Experiment (TOGA COARE) field experiment. He thus suggested that the Zhang and McFarlane scheme is more realistic than Hack's in estimating wave forcing. Considering that the GWDC parameterization is activated in a model only when and where convective clouds exist, the spatial and temporal variations of parameterized gravity wave drag are strongly dependent upon those of convective activity. In this sense, a more realistic cumulus parameterization scheme is necessary.

The magnitude of wave momentum flux at source level is another difficult issue. Since the magnitude of cloud-top wave stress is directly related to the impact of wave drag in a numerical model, it should be validated. However, there are no global observations of gravity wave momentum flux, particularly those induced by convective sources at cloud top. Even though simulated cloud-top wave stress can be compared with observations from aircrafts or radiosondes and with results from cloud-resolving models, this is not straightforward for several reasons. First, there is great degree of uncertainty in estimating wave momentum flux using observational data (Vincent and Alexander 2000). In addition, observations are taken in a limited area (even for aircraft observations) so that direct comparison with results obtained using a GCM with a horizontal grid area of $\sim$40 000 km^2 may not be reliable. The intermittency of convective sources in the atmosphere makes the problem much more complicated than in the case of mountain drag. Comparison with cloud-resolving model results raises a similar issue because detailed information on spatial and temporal variations of mesoscale convective cells in a GCM grid box is not provided by cumulus parameterization schemes used in most current GCMs. Convective clouds in most cumulus parameterization schemes are in a quasi-equilibrium state, whether they are described as a cloud ensemble or as a single cloud in a horizontal grid box. Gravity waves generated by these quasi-equilibrium clouds may be best represented to be stationary relative to the ground. Considering that nonstationary gravity waves can be generated largely by mesoscale convective cells propagating relative to a quasi-stationary convective system (Song et al. 2003), parameterizing nonstationary waves with the aid of a current cumulus parameterization scheme seems to be unnecessary. In order to include nonstationary waves in GCMs in a consistent way (i.e., coupled with other fields) rather than by specification, cumulus parameterization schemes must have a certain degree of realism that allows for a wide spectrum of gravity waves without any theoretical inconsistency.

Despite the issues mentioned earlier, the current study clearly demonstrates that the parameterization of convectively forced gravity wave drag proposed by Chun

and Baik (1998) significantly influences the zonal-mean wind and temperature fields in the tropical upper troposphere and stratosphere, which successfully alleviates the systematic model biases of CCM3.

Acknowledgments. The authors would like to thank two anonymous reviewers for their comments that helped improve the manuscript. The first author (HYC) also would like to thank Dr. Tim Dunkerton for discussion about the secondary circulation induced by gravity wave drag in the early stage of the work. The first (HYC) and the second (ISS) authors were supported by Korean Research Foundation Grant (KRF-2002-DS0076). The third author (JJB) was supported by the Climate Environment System Research Center sponsored by the SRC Program of the Korea Science and Engineering Foundation and also by the Brain Korea 21 Program. The last author (YJK) was supported by the Office of Naval Research under ONR Program Element 0602435N.

REFERENCES

Alexander, M. J., and L. Pfister, 1995: Gravity wave momentum flux in the lower stratosphere over convection. *Geophys. Res. Lett.,* **22,** 2029–2032.

——, and J. R. Holton, 1997: A model study of zonal forcing in the equatorial stratosphere by convectively induced gravity waves. *J. Atmos. Sci.,* **54,** 408–419.

——, and T. J. Dunkerton, 1999: A spectral parameterization of mean-flow forcing due to breaking gravity waves. *J. Atmos. Sci.,* **56,** 4167–4182.

Andrews, D. G., J. R. Holton, and C. B. Leovy, 1987: *Middle Atmosphere Dynamics.* Academic Press, 489 pp.

Chun, H.-Y., and J.-J. Baik, 1998: Momentum flux by thermally induced internal gravity waves and its approximation for large-scale models. *J. Atmos. Sci.,* **55,** 3299–3310.

——, and ——, 2002: An updated parameterization of convectively forced gravity wave drag for use in large-scale models. *J. Atmos. Sci.,* **59,** 1006–1017.

——, M.-D. Song, J.-W. Kim, and J.-J. Baik, 2001a: Effects of gravity wave drag induced by cumulus convection on the atmospheric general circulation. *J. Atmos. Sci.,* **58,** 302–319.

——, I.-S. Song, and M.-D. Song, 2001b: Effects of gravity wave drag induced by convection (GWDC) on the atmospheric general circulation simulated by YONU AGCM. *J. Korean Meteor. Soc.,* **37,** 347–366.

Dunkerton, T., and D. Delisi, 1985: Climatology of the equatorial lower stratosphere. *J. Atmos. Sci.,* **42,** 376–396.

Fovell, R., D. Durran, and J. R. Holton, 1992: Numerical simulations of convectively generated stratospheric gravity waves. *J. Atmos. Sci.,* **49,** 1427–1442.

Fritts, D. C., 1984: Gravity wave saturation in the middle atmosphere: A review of theory and observations. *Rev. Geophys. Space Phys.,* **22,** 275–308.

——, and W. Lu, 1993: Spectral estimates of gravity wave energy and momentum fluxes. Part II: Parameterization of wave forcing and variability. *J. Atmos. Sci.,* **50,** 3695–3713.

Gates, W. L., 1992: AMIP: The Atmospheric Model Intercomparison Project. *Bull. Amer. Meteor. Soc.,* **73,** 1962–1970.

Giorgetta, M. A., E. Manzini, and E. Roeckner, 2002: Forcing of the quasi-biennial oscillation from a broad spectrum of atmospheric waves. *Geophys. Res. Lett.,* **29,** 1245, doi:10.1029/2002GL014756.

Gregory, D., R. Kershaw, and P. M. Inness, 1997: Parameterization of momentum transport by convection. II: Tests in single-column and general circulation models. *Quart. J. Roy. Meteor. Soc.,* **123,** 1153–1183.

Hack, J. J., 1994: Parameterization of moist convection in the National Center for Atmospheric Research Community Climate Model (CCM2). *J. Geophys. Res.,* **99,** 5551–5568.

——, J. T. Kiehl, and J. W. Hurrell, 1998: The hydrologic and thermodynamic characteristics of the NCAR CCM3. *J. Climate,* **11,** 1179–1206.

Hamilton, K., R. J. Wilson, and R. S. Hemler, 1999: Middle atmosphere simulated with high vertical and horizontal resolution versions of a GCM: Improvements in the cold bias and generation of a QBO-like oscillation in the Tropics. *J. Atmos. Sci.,* **56,** 3829–3846.

Hines, C. O., 1991: The saturation of gravity waves in the middle atmosphere. Part II: Development of Doppler-spread theory. *J. Atmos. Sci.,* **48,** 1360–1379.

Holton, J. R., 1982: The role of gravity wave induced drag and diffusion in the momentum budget of the mesosphere. *J. Atmos. Sci.,* **39,** 791–799.

Horinouchi, T., 2002: Mesoscale variability of tropical precipitation: Validation of satellite estimates of wave forcing using TOGA COARE radar data. *J. Atmos. Sci.,* **59,** 2428–2437.

Hurrell, J. W., J. J. Hack, B. A. Boville, D. L. Williamson, and J. T. Kiehl, 1998: The dynamical simulation of the NCAR Community Climate Model Version 3 (CCM3). *J. Climate,* **11,** 1207–1236.

Kanamitsu, M., W. Ebisuzaki, J. Woollen, S.-K. Yang, J. J. Hnilo, M. Fiorino, and G. L. Potter, 2002: NCEP–DOE AMIP-II reanalysis (R-2). *Bull. Amer. Meteor. Soc.,* **83,** 1631–1643.

Kershaw, R., 1995: Parameterization of momentum transport by convectively generated gravity waves. *Quart. J. Roy. Meteor. Soc.,* **121,** 1023–1040.

Kiehl, J. T., J. J. Hack, G. B. Bonan, B. A. Boville, B. P. Briegleb, D. L. Williamson, and P. J. Rasch, 1996: Description of the NCAR Community Climate Model (CCM3). Tech. Note NCAR/TN-420+STR, Boulder, CO, 152 pp.

Kim, Y.-J., 1996: Representation of subgrid-scale orographic effects in a general circulation model. Part I: Impact on the dynamics of simulated January climate. *J. Climate,* **9,** 2698–2717.

——, S. D. Eckermann, and H.-Y. Chun, 2003: An overview of the past, present and future of gravity-wave drag parameterization for numerical climate and weather prediction models. *Atmos.–Ocean,* **41,** 65–98.

Lindzen, R. S., 1981: Turbulence and stress owing to gravity wave and tidal breakdown. *J. Geophys. Res.,* **86,** 9707–9714.

Lott, F., and M. J. Miller, 1997: A new subgrid-scale orographic parameterization: Its formulation and testing. *Quart. J. Roy. Meteor. Soc.,* **123,** 101–127.

McFarlane, N. A., 1987: The effect of orographically excited gravity wave drag on the general circulation of the lower stratosphere and troposphere. *J. Atmos. Sci.,* **44,** 1775–1800.

Medvedev, A. S., and G. P. Klaassen, 1995: Vertical evolution of gravity wave spectra and the parameterization of associated wave drag. *J. Geophys. Res.,* **100,** 25 841–25 853.

Palmer, T. N., G. J. Shutts, and R. Swinbank, 1986: Alleviation of a systematic westerly bias in general circulation and numerical weather prediction models through an orographic gravity wave drag parameterization. *Quart. J. Roy. Meteor. Soc.,* **112,** 1001–1039.

Piani, C., D. Durran, M. J. Alexander, and J. R. Holton, 2000: A numerical study of three-dimensional gravity waves triggered by deep tropical convection and their role in the dynamics of the QBO. *J. Atmos. Sci.,* **57,** 3689–3702.

Pierrehumbert, R. T., 1986: An essay on the parameterization of orographic gravity wave drag. *Proc. Seminar/Workshop on Observation, Theory and Modeling of Orographic Effects,* Vol. 1, Reading, United Kingdom, ECMWF, 251–282.

Ricciardulli, F., and R. R. Garcia, 2000: The excitation of equatorial

waves by deep convection in the NCAR Community Climate Model (CCM3). *J. Atmos. Sci.,* **57,** 3461–3487.

Rind, D., R. Suozzo, N. K. Balachandran, A. Lacis, and G. Russell, 1988: The GISS global climate–middle atmosphere model. Part I: Model structure and climatology. *J. Atmos. Sci.,* **45,** 329–370.

Sato, K., and T. J. Dunkerton, 1997: Estimates of momentum flux associated with equatorial Kelvin and gravity waves. *J. Geophys. Res.,* **102,** 26 247–26 261.

Scaife, A. A., N. Butchart, C. D. Warner, and R. Swinbank, 2002: Impact of a spectral gravity wave parameterization on the stratosphere in the Met Office Unified Model. *J. Atmos. Sci.,* **59,** 1473–1489.

Shutts, G. J., 1995: Gravity-wave drag parameterization over complex terrain: The effect of critical-level absorption and directional wind-shear. *Quart. J. Roy. Meteor. Soc.,* **121,** 1005–1021.

Song, I.-S., H.-Y. Chun, and T. P. Lane, 2003: Generation mechanisms of convectively forced internal gravity waves and their propagation to the stratosphere. *J. Atmos. Sci.,* **60,** 1960–1980.

Swinbank, R., and A. O'Neill, 1994: A stratosphere–troposphere data assimilation system. *Mon. Wea. Rev.,* **122,** 686–702.

Vincent, R. A., and M. J. Alexander, 2000: Gravity waves in the tropical lower stratosphere: An observational study of seasonal and interannual variability. *J. Geophys. Res.,* **105,** 17 971–17 982.

Warner, C. D., and M. E. McIntyre, 1999: Toward an ultra-simple spectral gravity wave parameterization for general circulation models. *Earth Planets Space,* **51,** 475–484.

Wu, X., and M. Moncrieff, 1996: Collective effects of organized convection and their approximation in general circulation models. *J. Atmos. Sci.,* **53,** 1477–1495.

Zhang, G. J., and N. A. McFarlane, 1995: Sensitivity of climate simulations to the parameterization of cumulus convection in the Canadian Climate Center general circulation model. *Atmos.–Ocean,* **33,** 407–446.

Zwiers, F. W., and G. J. Boer, 1987: A comparison of climates simulated by a general circulation model when run in the annual cycle and perpetual modes. *Mon. Wea. Rev.,* **115,** 2626–2644.